Public domain. CC0 1.0.





Hazard Potential of Compound Flooding from Rainfall, Storm Surge, and Groundwater in Coastal New York and Connecticut

Robin Glas¹, Liv Herdman¹, Salme Cook¹, Archi Howlader², Kristina Masterson¹

- ¹ U.S. Geological Survey, New York Water Science Center, Troy, NY, USA
- ² Akima Systems Engineering, Contractor to the U.S. Geological Survey, now at Kansas Geological Survey, Lawrence, KS, USA

Correspondence to: Robin Glas (rglas@usgs.gov)

Short Summary

We analyzed long-term groundwater, precipitation, and storm-surge records across coastal New York and Connecticut to estimate how often these hazards occur together. Overlap is highest along southwestern Long Island and western coastal Connecticut during the colder months, when groundwater is higher and mid-latitude cyclones are more common. Results from this study can support better preparation for coastal storms by taking into consideration the compounding effects of different flood drivers.

15 Abstract

Compound flood events, defined here as the co-occurrence of more than one flood type, can result in flood hazard potential that is higher than if the events occurred independently. To evaluate compound flooding in a semi-urbanized coastal area, historical records dating back to 1970 are used to study the co-occurrences of high precipitation, storm surge, and shallow groundwater conditions for Long Island and the Long Island Sound vicinity across coastal New York and Connecticut. Joint return periods for coincident precipitation-surge events were computed using fitted copulas and compared to the assumption of independence as a ratio of return periods, referred to here as a return period adjustment. Results indicate distinct seasonality where compound events in the area disproportionately occur in the cold season between October and April. Return period shifts range from 1 to almost 9, demonstrating the range in precipitation-storm surge dependence across the study area. Across all 24 station triad locations, groundwater levels were elevated during times of precipitation-storm surge co-occurrence, in areas where the average depth to water is shallow (less than 20 feet or 6 m below land surface). The result is a pseudo-trivariate compound flood potential map that integrates dependence between daily

Public domain. CC0 1.0.





precipitation-surge events and overall monthly groundwater levels into a relative compound hazard score. The location with the highest compound flood hazard score is in the south shore of Long Island, as well as locations across coastal Connecticut where groundwater levels are already near-surface during events where both heavy rainfall and high coastal storm surge occur at the same time.

1 Introduction

Coastal compound flooding, defined herein, is the concurrent or close succession of high precipitation and storm surge, and such flooding poses substantial challenges to communities along the East Coast of the United States (Nederhoff et al., 2024; Wahl et al., 2015). Coastal compound events have led to devastating impacts, resulting in loss of life (Hanchey et al., 2021), damage to property and infrastructure, and long-term economic effects (Green et al, 2024). Ghanbari et al. (2021) concluded that in recent years, the frequency and intensity of compound flooding have become more pronounced, exacerbated by climate change and sea level rise, highlighting the urgent need for refined risk assessments and mitigation strategies. Compound events, such as Tropical Storm Irene in 2011 and a historically important Nor'easter (colloquial regional meteorologic term for extra-tropical cyclones) in March 2010, caused wide-spread damage across the metropolitan area of the City of New York (hereafter "New York City"), with elevated storm tides and heavy precipitation occurring on top of soils that were already saturated or covered with antecedent snow (Orton et al., 2012).

This study focuses on compound coastal flood events and their geographic distribution around New York City, Long Island, and Long Island Sound, leveraging multiple historical records from precipitation stations, tidal gauges, and groundwater records spanning the past half-century. Previous studies have examined the occurrence of concurrent precipitation and surge events in this region utilizing tidal gauge data centred on a few stations near New York City, Montauk, N.Y., New London, Conn., and Bridgeport, Conn., for various data lengths and periods of record (e.g., Chen et al., 2024; Ghanbari et al., 2021; Nasr et al., 2023; Wahl et al., 2015). These studies indicate weak, positive dependences between storm surge levels and either precipitation or river discharge. The dependence of coastal storm surge between either precipitation depth or river discharge may be increasing in magnitude for hydrometeorological stations along the U.S. East Coast with teleconnections to climate

Public domain. CC0 1.0.





indices such as the Arctic Oscillation (Nasr et al., 2023). These previous studies have laid the groundwork for understanding the impacts of compound coastal events, and this study aims to enhance the existing body of knowledge by providing a higher spatial resolution analysis reviewing the geographic effects of proximity to the U.S. mainland and Long Island Sound on compound flood occurrence and groundwater conditions during these events.

Using copula models, the dependence between precipitation and storm surge for 24 precipitation-tidal station pairs are assessed across the study area. Copulas have been shown to be suitable statistical tools for understanding the relations between multi-dimensional random variables, particularly in the context of hydrological events (Salvadori and De Michele, 2007; 2010). Using a copula approach, the dependence between two or more continuous variables can be uniquely modelled independent of the marginal distributions, and multivariate nonexceedance probabilities can be computed for event pairs in more than one dimension (Favre et al., 2004). These nonexceedance probabilities can be expressed as bivariate return periods, most commonly for the OR case, where at least one variable exceeds a desired threshold, or for the AND case, where both variables are considered extreme (Brunner et al., 2016; Salvadori, 2004; Shiau, 2003). In this study, we consider the AND scenario when both precipitation and storm surge are simultaneously at their high concurrent levels.

Sea level rise, precipitation increases, and aging drainage infrastructure put shorelines at risk for more pronounced groundwater emergence, especially in coastal urban areas (Bosserelle et al., 2022). The coastlines of New York and Connecticut are discharge areas for the unconfined groundwater flow system characterized by shallow depths to groundwater and a high proportion of urban development (Rosenzweig et al., 2024). Groundwater flooding across heavily urbanized coastal areas will likely be exacerbated by sea level rise, in particular where the water table is no longer depressed because groundwater pumping has since ceased and where land filling practices have placed modern buildings and infrastructure over what used to be wetlands and drainage channels (Su et al., 2022; Bosserelle et al., 2022. Unconfined depth to water can be relatively shallow across coastal New York City, Long Island, and southern Connecticut (Bjerklie et al., 2012) (refer also to https://ny.water.usgs.gov/maps/lidtw/ [accessed March 17, 2025]). We examine the occurrence of precipitation-storm surge compound events with shallow depths to water using historical groundwater data across the study area. The

Public domain. CC0 1.0.



85

100

105

110



interaction between these three factors can better inform the risk landscape for coastal communities during extreme weather events.

To illustrate the relative frequency of compound flood hazard across the New York City-Long Island-Long Island Sound region, comprehensive maps are presented that depict the spatial variations in the strength of dependence between precipitation and storm surge, along with the occurrence of shallow groundwater during these compound events. By describing the geographic distribution and interplay of flood drivers, this research furthers understanding of coastal compound flooding across coastal New York and Connecticut, to help inform stakeholders and decision makers about hydrologic hazards.

2 Study Area

The study area encompasses the densely populated coastal region along the northeastern United States, specifically focusing on Long Island (including the majority of New York City), and the northern shoreline of Long Island Sound, comprising the southern coast of Connecticut. People and property in this region have faced challenges from aging flood protection and drainage infrastructure (Forman, 2014), exposure to severe coastal flooding and erosion (Fallon and Kuonen, 2023), pronounced increasing trends in both extreme and annual precipitation (Kunkel et al., 2020), and sea level rise of approximately 10 cm over the past century that can be directly attributed to anthropogenic climate change and associated flood damages from tropical cyclones (Herreros-Cantis et al., 2020; Strauss et al., 2021).

Densely populated Long Island, New York extends approximately 120 miles (193 km) eastward from New York City to Montauk Point and comprises four counties: Kings (Brooklyn), Queens, Nassau, and Suffolk. With a population exceeding 7.8 million (U.S. Census Bureau, 2023), Long Island has development along much of the coastline. Groundwater dynamics of Long Island are influenced by its stratified aquifer system, primarily composed of sand and gravel that allows for efficient drainage and groundwater recharge (Walter and others, 2024). Areas where the depth to groundwater is shallow are vulnerable to flooding during heavy precipitation (Glas et al., 2023; Suffolk County, 2020).

Long Island has been impacted by devastating storms, with named storms including Tropical Storm Irene (2011) and Post-Tropical Cyclones Sandy (2012), and Ida (2021) having inflicted wide-

Public domain. CC0 1.0.



115

125

130

135



spread damage across the region from heavy rainfall (localized flooding for areas lacking sufficient drainage), record breaking storm surges, and basement flooding (a basement being a floor or level of a structure that is below the ground level). Whereas these tropical storms have garnered substantial attention because their intensity, areal-wide presence, and impacts, it is the more moderate extratropical cyclones that have been both more frequent and widespread, resulting in recurring flooding and storm surge events that affect a larger area (Booth et al., 2016; Liu et al., 2020). The combination of Long Island's exposure to cyclonic storm tracks and topography, low-lying coastal areas and marshes, along with intensive urban development make the region vulnerable to compound flooding, thereby drawing attention to water-management practices and coastal resilience planning (Rosenzweig et al., 2024. In particular, the southern shore is susceptible to flooding because of its shallow depth to groundwater, and exposure to storm tracks originating both from the U.S. mainland and the open Atlantic Ocean (Glas et al., 2023; Shepard et al., 2012).

Long Island Sound is a semi-enclosed tidal estuary located between Long Island, New York, and the southern coast of Connecticut, characterized by complex bathymetry and geography that substantially influence its susceptibility to coastal flooding (Liu et al., 2020). The relatively shallow depths of Long Island Sound (averaging about 60 feet, 18 m) allow for the amplification of storm surges (Kouhi et al., 2022; Wong, 1990), particularly during intense weather events, as observed during both tropical and extratropical storms (Booth et al., 2016; DeGaetano, 2008). Across the west-to-east gradient of Long Island Sound, storm generating mechanisms contribute to the severity of storm surge impacts, with extratropical cyclones causing the highest and most frequent surges in the western end of the sound, while tropical storms and hurricanes create the largest surges in the eastern part near the open ocean (O'Donnell and O'Donnell, 2012).

3 Data and Methods

3.1 Station selection and missing-record imputation

A total of 275 observing stations were considered for this study, located across the study area that includes the coasts or coastal regions of New York City, Long Island, and Long Island Sound (Fig. 1). Three data types were used in this analysis: (1) daily precipitation totals, (2) daily coastal non-tidal

Public domain. CC0 1.0.



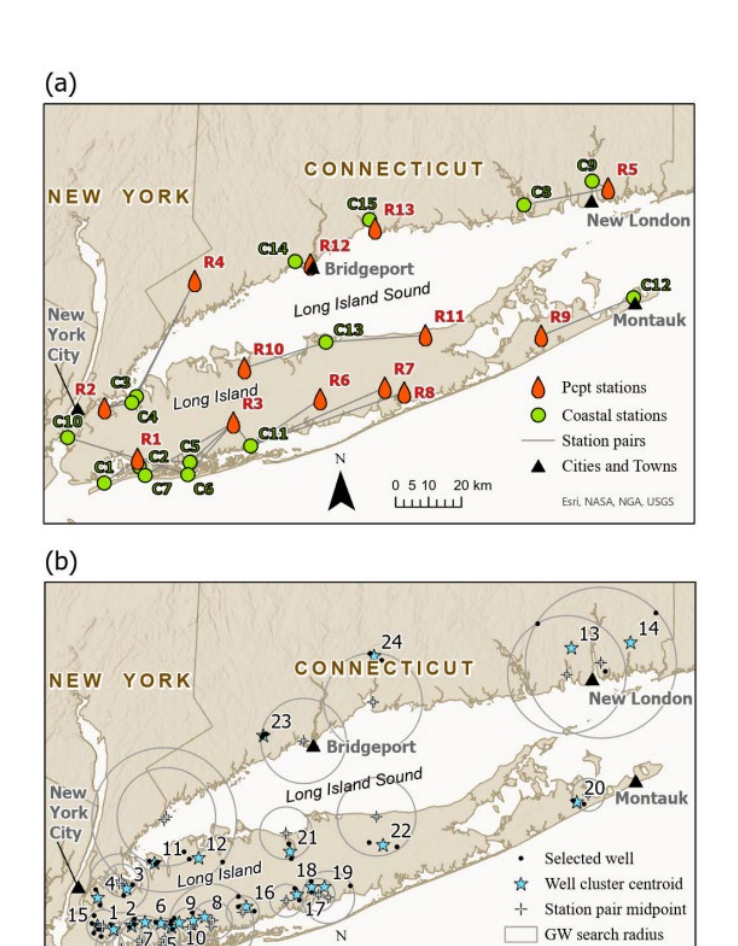


residuals representing storm surge, and (3) observed monthly groundwater levels measured in the uppermost unconfined hydrogeologic unit near the coast. First, total calendar day (24 hour)

precipitation values were retrieved from 21 National Oceanic and Atmospheric Administration (NOAA) precipitation observing stations (NOAA NCEI, 2023) for a 52-year period spanning calendar years 1970 through 2021. On days when precipitation fell as snow, the liquid water equivalent was used as the







0 5 10 20 km

Figure 1. (a) Locations of precipitation, coastal water level, and groundwater observation stations used in the analysis; additional site information is provided in table 1. (b) Station triad locations, plotted at the nearest land point to the centroid of each triad composed of a precipitation gage, a coastal water level station, and a cluster of groundwater observation wells. Precipitation/surge midpoints are shown as the geographic midpoint between each precipitation and coastal station pair, with circular search radii indicating the area within which groundwater wells were selected for inclusion in each triad. Projection World Geodetic System of 1984, Base modified from U.S. Geological Survey digital data, 1:1,200,000.

Cities and Towns

Esri, NASA, NGA, USGS

precipitation value for that day as provided in the associated daily NOAA data report. Second, coastal water levels were retrieved from 12 NOAA water-level stations (NOAA CO-OPS, 2023) with recorded hourly water levels (meters) and 22 U.S. Geological Survey (USGS) water-level stations (<u>U.S.</u> Geological Survey, 2023) with recorded 15-minute water levels that have record lengths longer than 9.9

Public domain. CC0 1.0.



155

160

165

170



years between 1970 and 2021. A 33-hour low pass filter was applied to the observed hourly water level time series to compute the non-tidal residual (NTR), which is conceptually akin to "storm surge". The computed NTRs were subsampled to daily maximum values. Third, monthly groundwater levels were retrieved using the USGS National Water Information System (NWIS; <u>U.S.</u> Geological Survey, 2023) for 220 unconfined observation wells throughout Long Island, New York City, and southern Connecticut for the calendar years 1975 through 2021. A starting year of 1975 for groundwater optimized the imputation quality based on data availability. Table 1 contains all station identification numbers, locations, and map I.D.s linking station locations to the maps in Fig. 1.

Some real-time groundwater monitoring networks are available on Long Island at daily temporal resolution (U.S. Geological Survey, 2023) and can be used to analyse the response of groundwater to compound coastal flooding. However, the monitoring frequency is monthly for many wells with longer periods of record in Long Island, New York City, and Southern Connecticut.

Missing values for each of the three data types were filled using neighbouring, correlated stations at a daily timestep for precipitation and NTR, and at a monthly timestep for groundwater. The imputations were carried out using the ARCHI R package (Levy et al., 2024, R Core Team, 2024, version 4.4.1), which iteratively searches the available input data for multiple correlated reference stations and uses regression to predict missing values at the target station. Each of the three data types were imputed using the ridge regression option within ARCHI, except for the case where only one reference station was available, and in that case simple linear regression was used. A Pearson correlation coefficient of 0.6 and a Nash–Sutcliffe Efficiency (NSE) of 0.4 were used as the minimum threshold for accepted regression models in the ARCHI algorithm. Special consideration was given to the precipitation dataset because predictions from the ARCHI algorithm sometimes included near-zero negative values; predictions that were less than 1 mm were censored to zero. Full imputation statistics are shown in supplemental tables S1, S2, and S3. To further evaluate imputation quality, five percent of the observed values for each of the three data types were withheld (daily precipitation in millimeters, daily storm surge as NTR in meters, and monthly groundwater in feet below land surface), including separate consideration of wet day (observed prep> 1 mm) and dry day (observed prep < 1 mm)



185

190

200



precipitation. The ARCHI algorithm then imputed those values and were compared to the observed values by root mean squared error (RMSE) and bias (percent).

Using the complete imputed data records, 24 precipitation-coastal station pairs were selected based on proximity and unique paired combinations. Groundwater observation wells were selected using a cluster-based approach centered on the midpoint between each precipitation/coastal station pair. Beginning with a 5-km search radius around each midpoint, wells were selected based on the following criteria: (1) at least 90% data availability from 1975 to 2021 in the imputed monthly time series, (2) 100% data availability from 2010 to 2021 to capture recent extremes, and (3) a minimum observed depth to water less than 50 feet or 15 m below land surface (bls), to exclude deeper aquifer zones or wells not representative of near-surface conditions. If fewer than two qualifying wells were found within the 5-km radius, the radius was incrementally expanded until the criteria were met. A maximum of 10 wells per triad were retained. Final selections were manually reviewed to confirm hydrogeologic consistency within each cluster. Final station triad groups are listed in Table 1 and respective group centroids shown in Fig. 1b. A list of all the selected wells and their associated triads are listed in Supplemental table S4.

3.2 Precipitation-surge event sampling

To evaluate the relations between daily precipitation and storm surge, event pairs were selected and modeled using copulas with a "two-sided sampling approach" (Jane et al., 2022). Data were prepared for bivariate modeling by detrending coastal NTR (storm surge) values over a three-month moving window. No trends were detected in the daily precipitation time series. High or extreme events were identified in each dataset using a peaks-over-threshold (POT) approach, applying thresholds from the 90th to the 99th empirical quantile at each station. To ensure the selection of independent events, a separation window of 10 days for precipitation and 6 days for NTR was established, which aligns with the lag times for considering concurrent events: ±5 days for precipitation and ±3 days for surge (Agel et al., 2015; Barbot et al., 2024). Final POT thresholds were chosen to limit the number of independent events per year to between 3 and 6 while maximizing the Kendall tau correlation coefficient between the two variables.

210

To create two distinct biconditional datasets, the R package Multihazard (Jane et al., 2020) was used with the Multihazard::Con_Sampling_2D_Lag function. This process began with selecting 24-hour precipitation totals that exceeded the selected threshold, followed by identifying the maximum NTR occurring within three days of each precipitation event. We repeated this for all independent precipitation events and their corresponding surge events, considering a time window of ±5 days. The resulting datasets include one conditioning on precipitation (CoP) and another on surge (CoS). Time lags of 3 days for CoS and 5 days for CoP were used to associate each variable with the other. These time lags were based on findings that average coastal storm surge events around New York have durations that range from 1.6 to 3.3 days (Barbot et al., 2024), and that the most common duration for extreme rain events in coastal areas of the Northeast is between 2 and 5 days (Agel et al., 2015). This approach accommodates potential mismatches between peak rainfall and storm surge that still have overlapping events, as well as delays in water reaching the coast via overland flow.

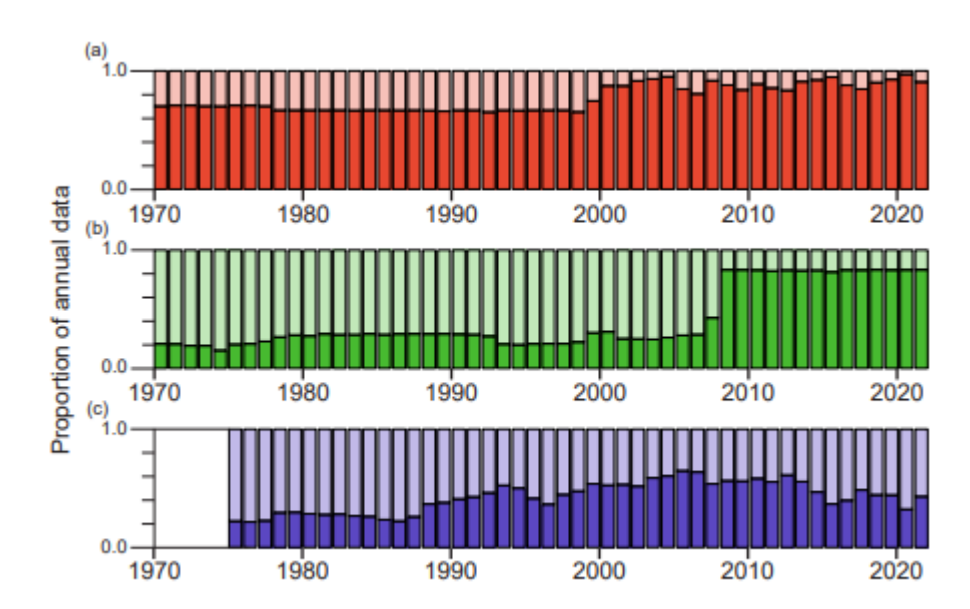


Figure 2. Proportion of observed (dark shading) and imputed (light shading) time steps for each calendar year. (a) Precipitation data (red; daily), (b) coastal non-tidal residual (NTR) data (green; daily), and (c) groundwater data (purple; monthly).



220

225

235



3.3 Precipitation-surge dependence

Biconditional precipitation-surge event sets were assessed for correlation using Kendall tau for each triad. To identify temporal changes in this correlation structure, 20-year moving windows were used to re-compute the Kendall tau for selected events inside that time window, then shifted by one year across the time range of the dataset. To evaluate temporal changes in dependence structure, the empirical upper tail dependence coefficient ($\widehat{\lambda_U}$ hereafter referred to as uTDC) was computed separately for the first and second halves of the study period. The uTDC was estimated using the following formula:

$$\widehat{\lambda_U} = \frac{1}{n_u} \sum_{i=1}^n I(U_i > u, V_i > u)$$

where U_i and V_i are pseudo-observations on the unit interval, I is the indicator function, and n_u is the number of observations exceeding the threshold u. Estimates were computed for u=0.6, representing the upper half of the distribution, and u=0.9, representing the upper tail. Calculations were performed for the periods 1975–1995 and 1996–2021 to assess changes in upper tail dependence over time and evaluate the need for a nonstationary framework.

To model the dependence structure in the data, each feature in the biconditional datasets was transformed into a uniform distribution by computing their rank-based pseudo-observations. The pseudo-observations are "plotting positions" using common nomenclature in hydrologic hazards (Asquith and others, 2017, app. 2), lie on [0,1], and correspond to the data mapped to rank-based cumulative probability space. An independence test of the pseudo-observation pairs was completed before selecting a copula model, where the null hypothesis is bivariate independence using the R function VineCopula::BiCopIndTest (Nagler et al., 2023, Genest and Favre, 2007). In the cases where the pseudo-observations are quantitively independent (p-value > 0.05), then the independence copula was selected for those station pairs. For bivariate data pairs exhibiting statistically significant dependence, parametric copula models were fitted using maximum likelihood estimation. The candidate set included two elliptical copulas: Gaussian and t, and three Archimedean copulas: survival Clayton, Gumbel, and Frank. These six copulas were selected to capture a range of tail dependence structures relevant to the variables of interest (rainfall and NTR). Specifically, survival Clayton and Gumbel

Public domain. CC0 1.0.



245

255

260

265



exhibit upper tail dependence, the t copula exhibits symmetric tail dependence (both upper and lower), and the Gaussian and Frank copulas are tail-independent. These copulas are relatively common tools for practitioners and are all permutation symmetric, which means for the copula C(u,v) that C(v,u) = C(u,v). Such symmetry is therefore an implicit assumption for this study.

The best fitting copula was selected using the minimum Akaike information criterion (AIC, Akaike, 1973; Asquith and others, 2017, app. 4). The AIC offers a comparative measure of fit for candidate copulas, identifying the model with the lowest AIC as the optimal choice. In instances where the difference in AIC between the top candidate and the next best model was less than 2 (ΔAIC<2), indicating a statistical tie in support, an additional screening was performed. Specifically, the empirical upper tail dependence coefficient (uTDC) of the observed data was compared against the distribution of uTDC values derived from 500 bootstrap simulations of each candidate model. If the absolute difference between the empirical uTDC and the median of the simulated uTDCs exceeded 0.1, the model was considered to provide a poor approximation of tail behavior and was excluded from consideration. The remaining model with the better agreement in uTDC was selected.

Graphical diagnostics and a goodness-of-fit hypothesis test were used to assess absolute fit and ensure that the selected model adequately represents the raw data. The quality of fit was graphically inspected by comparing the fitted parametric copula to the empirical copula by contour lines along cumulative probability values (the "level curves" in copula nomenclature, not shown). Additionally, a rank-based goodness-of-fit test was applied to further assess the fit of the selected copulas (Huang and Prokhorov, 2014). This test is semi-parametric, using a parametric copula and nonparametric, empirical marginals where the null hypothesis pertains to the assumption of the data following the specified copula model using the VineCopula::BiCopGofTest function in the VineCopula R package (Nagler et al., 2023).

When computing return periods for bivariate data using copulas, there are an infinite number of data pairs (precipitation-surge) associated with a single joint return period that can be graphically represented by contour lines instead of univariate singular estimates. Return period contour lines associated with each biconditional dataset were computed using the fitted copula through Eq. 2 for the

Public domain. CC0 1.0.



270

275

280

285

290



AND joint return period, examining the probability of a specific magnitude of precipitation and coincident surge:

$$RP_{AND} = \frac{\mu}{1 - u - v + C(u, v)}$$

where μ is the average interarrival time of events in years, and u and v are the marginal cumulative distribution functions (CDFs) associated with each variable, and C(u,v) is the joint CDF of the selected copula function. Under the assumption of independence, the joint AND return period is the product of the two marginal return periods, incorporating their respective exceedance probabilities. In contrast, under dependence, this relation is altered, and for positively correlated variables, the joint AND return period is shorter than under the independence assumption.

For each triad, and for the subset of univariate marginal return periods of 2, 10, 25, 50, and 100 years for both precipitation and surge, the ratio of the bivariate AND return period under independence to the dependence case was calculated for each combination of univariate return periods using the selected copula model. This ratio of return periods, or return period adjustment, represents the degree of dependence between the variables across each unique combination of univariate return periods (Fx and Fy), allowing the measure of dependence between the variables to be assessed in units of return period (Zscheischler and Seneviratne, 2017).

3.4 Precipitation-surge compounding and uncertainty

To simplify the suite of return period adjustments across the unique Fx and Fy combinations, the array of return period adjustments was collapsed to a single value by weighted averaging. For each triad location, the paired events were randomly sampled 500 times with replacement, preserving pair structures and number of bivariate events. Copula parameters were re-estimated while maintaining the copula family type of the full dataset, and bivariate return periods and their corresponding adjustments from the independence case were re-computed. From the resulting distribution of return period adjustments corresponding to each unique pair of univariate marginal return periods, the 0.025 and

Public domain. CC0 1.0.



305

310



295 0.975 quantiles were extracted and used as 95% confidence intervals around each return period adjustment. The width of the 95% confidence interval is representative of bivariate sampling uncertainty around the return period adjustment calculations, and the inverses of these widths were used as weights in the final weighted averages of return period adjustments for the CoP and CoS paired values for each station triad. This results in two weighted average return period adjustments per station triad.

3.5 Groundwater and composite score

For each triad, median monthly groundwater levels were computed from the selected wells within each associated cluster. These monthly time series were linearly interpolated to daily resolution. Groundwater levels (in feet bls) were then extracted for the date of each event type: rainfall above threshold, surge above threshold, and concurrent rainfall/surge events. This extraction enabled assessment of groundwater conditions during different types of compound events. Because the groundwater levels may not have been measured during the actual storm event, the values used in this analysis may not represent the actual groundwater response to coastal and precipitation events.

To characterize groundwater-related hazard, the shallowest groundwater levels (minimum depth to water bls) were identified across the associated wells in each cluster, and their median was used to assign a groundwater hazard score. Median shallow depths ≤ 6 ft were assigned a score of 2 (high hazard), depths between 6 ft and 15 ft were scored as 1 (moderate hazard), and depths \geq 15 ft were scored as 0 (low hazard).

The groundwater hazard score was combined with two scores based on the dependence structure between precipitation and surge. First, a triad received 1 point if either CoP or CoS event datasets exhibited upper tail dependence, as determined by fitting a copula with upper tail dependence. Second, a triad received 1 point if symmetrical dependence was observed, meaning a non-independent copula was selected for both CoP and CoS event types.

The three component scores (groundwater depth, upper tail dependence, and dependence symmetry) were summed and rescaled to yield a final compound hazard score ranging from 1 (lowest) to 5 (highest) for each triad.

Public domain. CC0 1.0.



325

330

335

340

345



To interpolate these results across the entire study area (the coasts of Long Island Sound and the south shore of Long Island), each groundwater centroid location was initially assigned to one of eight clusters using *k*-means clustering (MacQueen, 1967), implemented with the scikit-learn Python library (Pedregosa et al., 2011). Clustering was based on the following six features: (1) average return period shift conditioned on precipitation (CoP), (2) average return period shift conditioned on surge (CoS), (3) median minimum groundwater depth (in feet), (4) groundwater hazard score, (5) biconditional dependence score, and (6) upper tail dependence score. To ensure spatial contiguity, stations that were grouped into non-contiguous clusters were reassigned to new, spatially coherent clusters. This post-processing resulted in a total of 11 final clusters, each containing between one and four stations.

For each cluster, a centroid was calculated and used to generate Voronoi polygons (Aurenhammer, 1991) that partitioned the entire study area. Separate Voronoi tessellations were created for Connecticut (CT), and for the north and south shores of Long Island. Within each Voronoi polygon, 900-meter grid cells were assigned the average compound hazard score of the stations in the corresponding cluster. Averaging was then masked and restricted to 900-meter grid cells located within the coastal 100-year flood (0.01 annual exceedance probability) hazard extent for the study area, as defined by Welk et al. (2025b). This grid is the same grid used for rainfall hazard (Welk et al., 2025b), coastal flood hazard (Cook and Herdman, 2025), and groundwater hazard (Welk et al., 2025a) across the same study area, allowing for direct spatial comparison of hazard scores across variables. The spatially continuous hazard map is based on interpolation of results from discrete monitoring stations. These stations are assumed to be representative of broader conditions, but the map does not account for local variability in precipitation, coastal water levels, or groundwater depth at locations where no measurements were available.

4 Results

4.1 Imputation quality

A total of 21, 34, and 207 observing stations were used to fill in missing records for precipitation, coastal NTR, and groundwater, respectively. Then, a subset of these stations, 13 precipitation, 15 coastal, and 58 groundwater observing stations, were used after imputation for input to the copula models and the final combined compound flood hazard score. The proportions of observed

Public domain. CC0 1.0.



350

355

360

365

370



and imputed values are presented in Fig. 2 for these stations, separated by each year of record from 1970 through 2021. Precipitation data had more than 80% observed values throughout the study period, whereas observed values for coastal NTR averaged about 15% until 2008 and 80% through 2021. Observed data comprised about 20% of groundwater records for 1975–1990, after which the proportion of observed records increased to between 40% to 60%. Despite the high proportion of imputed values in the NTR and groundwater datasets, their strong intrinsic correlation and sufficient duration of overlap justified their inclusion. Precipitation data exhibited lower cross-correlation; however, at least 80% of precipitation values were observed in any given year of the study period, exceeding the proportion of observed values in the NTR and groundwater datasets. Errors (RMSE and bias) were higher than for coastal water levels or groundwater, reflecting the greater spatial and temporal variability of precipitation. However, because the precipitation record contained a high proportion of observed values, only a small fraction of the series was imputed, limiting the influence of these higher errors.

The accuracy of the regression imputation process was assessed using the results from the holdout analysis, comparing observed to imputed across precipitation, coastal NTR, and groundwater datasets (Table 2). Higher error and bias resulted from wet-day imputations from dry, where imputation on wet days were on average 1.5 mm lower than observed values, and dry-day imputations were on average 0.34 mm higher than observed (zero) values (Table 2). Taken as a whole, holdouts from the entire precipitation dataset were on average 0.08 mm lower than observed values. Corresponding RMSEs for each precipitation holdout dataset were highest for wet days, lowest for dry days, and approximately 4.5 mm for all precipitation days as a whole. The NTR and groundwater datasets were slightly under-predicted by the imputations; however, these errors were relatively small (less than 1/100 of a meter and foot, respectively). Full imputation statistics for the entire dataset (not withheld values) are provided in Tables S1–S3.





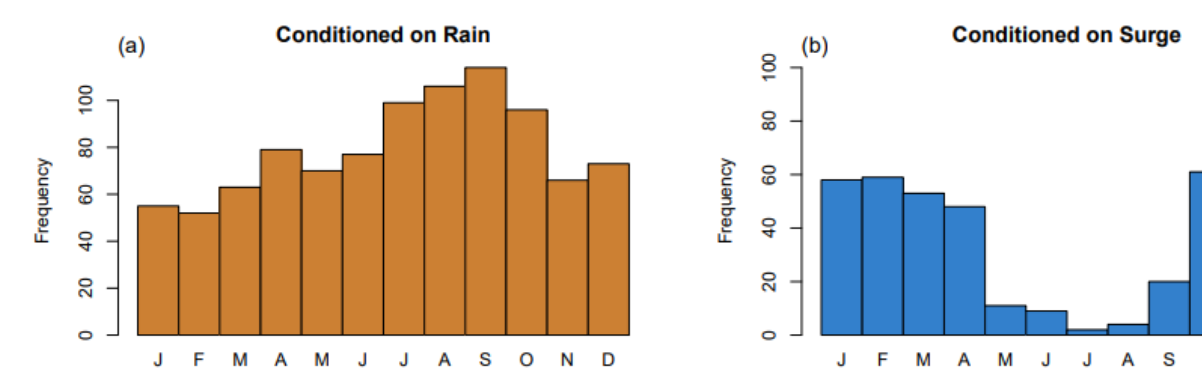


Figure 3. Monthly seasonality of unique concurrent events exceeding defined threshold quantiles, pooled across Triads 1 through 24. Events include rainfall/surge pairs selected from either (a) precipitation-conditioned (CoP) or (b) surge-conditioned (CoS) samples. Months are labeled on the x-axis by their first letter.

4.2 Biconditional sampling

375

380

Selected precipitation and surge threshold probabilities ranged from 0.97 to 0.99 across precipitation and surge datasets for all 24 triads (Table 3) and resulted in the average number events ranging from 3.1 to 5.8 events per year. Selected events conditioned on precipitation (CoP) showed a slightly seasonal pattern during the warmer months of the year, whereas events conditioned on surge (CoS) occurred distinctly between the months of October to April (Fig. 3). Sample size also varied across triads and sampling conditions, ranging from 162 (Triad 23, CoP) to 308 precipitation-surge events (Triad 22, CoP). Correlations across both datasets were weak, with higher and more substantial correlations when data were conditioned on surge. Mean Kendall tau of conditional datasets were 0.06 for CoP samples, and 0.13 for CoS samples. An example of data for Triad 15 (The Battery, NY) with selected precipitation and NTR thresholds is shown in Fig. 4.

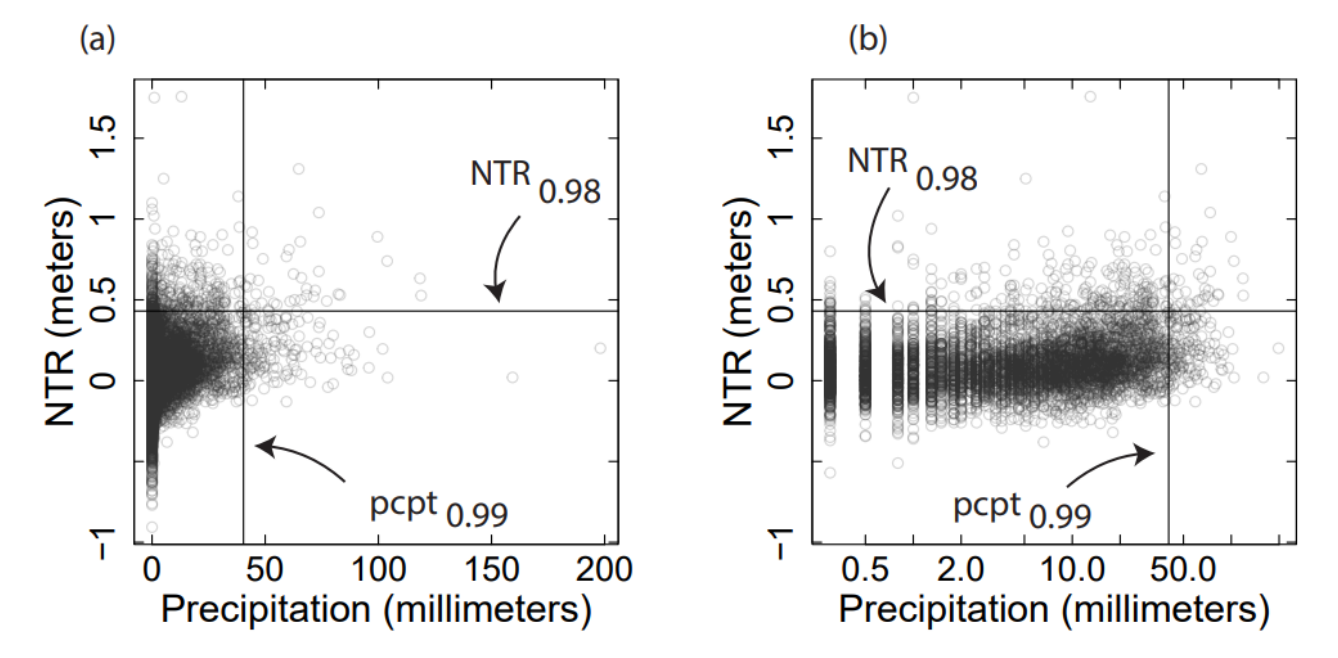


Figure 4. Daily precipitation and non-tidal residual (NTR) data for Triad 15 (Battery, NY), including selected fractional percentile thresholds for each variable. (a) Data shown in real space; (b) data shown on log-transformed axes with zero values excluded.



4.3 Dependence

Sampled events that were conditioned on surge showed more dependence than those conditioned on precipitation based on selected copula models. Independence was evident in 14 of the 24 triads where event selection was conditioned on precipitation, whereas only one of the triads (triad 10) was found to have independent data when events were conditioned on surge. For events conditioned on surge, 12 of 24 triads exhibited upper tail dependence (Table 4). Changes in Kendall tau for the period of study (1970–2021) were either slightly positive or slightly negative across all 24 triads but increased on average less than 0.1 over the study period (e.g., Triad 15, Fig. 5). Changes in the nonparametric

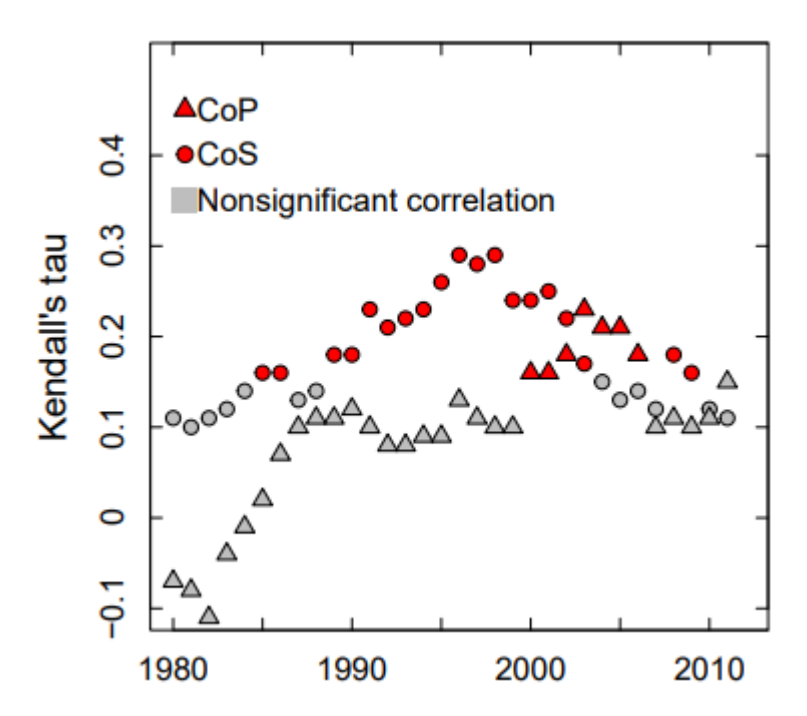


Figure 5. Time-varying Kendall correlations for Triad 15 (refer to Figure 1 for location), computed using a 20-year moving window shifted by one year. Correlations are based on selected precipitation/surge events under both sampling conditions: conditioned on precipitation (CoP) and conditioned on surge (CoS). Statistically significant correlations (p < 0.05) are shown in red.

upper tail dependence coefficient during the first half (1970–1995) to the second half (1996–2021) of



405



 $\triangle o$

0.05

the period evaluated in this study showed no persistently increasing or decreasing patterns across the 24 395 triads (Fig. 6). Based on these results, stationarity was assumed for this analysis.

For samples for which independence could not be ruled out, the independence copula was assigned; this explicit "snap" to independence means that reliance on a given nonindependent copula model with its empirical parameter was not made for this study (Table 4). Graphical comparison to the empirical copula (not shown), and p-values from the semi-parametric goodness-of-fit (GOF) test indicate the copula chosen by the AIC and uTDC criteria acceptably fit with the empirical data (pvalues for GOF test shown in Table 4). Model fit diagnostics for all candidate models are shown in Tables S5 and S6.

4.4 Precipitation- surge return period shifts

Figure 7 and Table 5 show and list, respectively, the results from the copula analysis as return period adjustments between the assumption of independence to dependence for concurrent

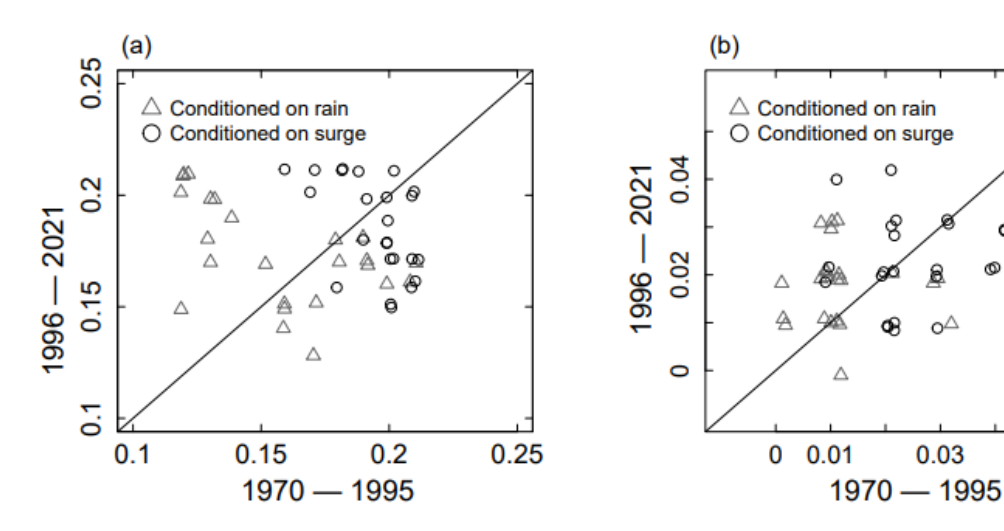


Figure 6. Empirical upper tail dependence coefficients (uTDC) computed at (a) u = 0.6 and (b) u = 0.9, corresponding to moderate and extreme upper-tail co-occurrence, respectively. Values are shown for the first (1970-1995) and second (1996–2021) halves of the record to assess potential nonstationarity in joint extremes. The diagonal line indicates the 1:1 (equal value) line. Points are jittered slightly to reduce overplotting.

Public domain. CC0 1.0.





precipitation-surge events. The weighted average return period adjustment encompasses all values across the selected univariate return period pairs, inversely weighted by the variability from the bootstrap resampling (Fig. 7). Because higher return period adjustments generally indicate more variability between the bootstrapped samples, the weights put more emphasis on shorter univariate return period events. Weighted average adjustments to return period due to the assumption of independence and dependence ranged from 1 (independent data) to 8.51 (triad 4, conditioned on surge, Table 5), meaning that coincident rain-surge events are more than eight times likely to occur when taking their dependence structure into account. The average return period adjustment conditioned on precipitation was 2.99, whereas the average adjustment conditioned on surge was 4.32 across all station triads. These return period adjustments correspond to copula models that exhibit upper tail dependence as well as statistically significant correlations represented in the Kendall's tau correlation coefficient (Tables 3 and 4).

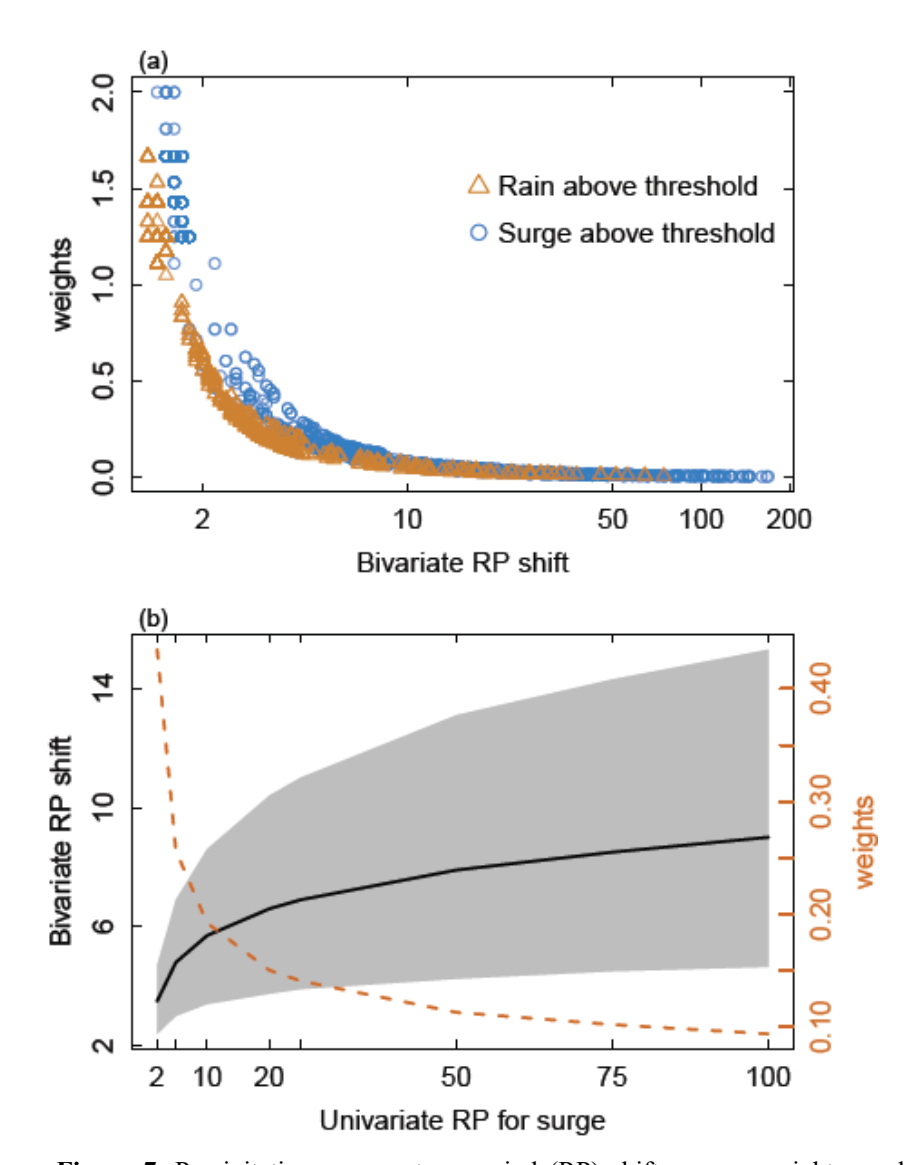


Figure 7. Precipitation—surge return period (RP) shifts versus weights used in the final averaging. (a) All triads combined. (b) Example of 95% confidence intervals for return period shifts corresponding to the 50-year univariate return period for rainfall, shown for Triad 15 at Battery, NY. Weights across univariate return periods shown in orange dashed line.

Public domain. CC0 1.0.



425

430

435



4.5 Groundwater and Multivariate rating score

Over the 1975–2021 period of data, the median shallowest (minimum) depth to groundwater was extracted for each station triad's cluster of groundwater wells (Table 5). Groundwater shallower than 6 feet or 1.8 m was associated with triads 16, 17, and 23 along the southern shore of Long Island and Connecticut, respectively. Depths to water between 6 and 10 feet (1.8 to 3 m) were found around the coastline of Long Island Sound at triads 11, 13, 14, and 24. Minimum groundwater depths less than 6 feet (1.8 meters) have the potential to interfere with drainage infrastructure, natural infiltration of soils, and may contribute to more overland runoff during precipitation events (Bosserelle et al., 2022). The spatial distribution of the median shallowest groundwater levels are shown in panel C of Fig. 9. Groundwater levels between 6 and 15 feet (1.8 to 4.5 m) will likely intersect with basements and other subsurface infrastructure (Conestoga-Rovers and Associates, 2007; New Jersey Department of Environmental Protection, 2021). During most precipitation-surge events, groundwater across the study area was elevated (more shallow) above median levels (Fig. 8). Because of the seasonal pattern of high storm surge, events that were sampled conditioned on surge occurred during the winter when regional groundwater storage and levels are highest (Bjerklie et al., 2012; Li et al., 2015).

Overall compound flood hazard rating was scored according to the criteria described in section 3.4, stratifying the scoring by magnitude of precipitation-surge return period adjustments and shallow (0 to 6 feet or 0 to 1.8 m) versus deeper (6 to 15 feet or 1.8 to 4.6 m) monthly average groundwater levels.

Final scores ranged from 1 to 5 and are generally higher (indicating higher compound flood risk) on the western south shore of Long Island, as well as along the Connecticut coast. Final compound hazard scores along with their scoring components are shown spatially in Fig. 10, plotted at the centroid of groundwater wells associated with each precipitation—coastal station pair. Interpolated results across the study area are shown in Fig. 10a and as a shapefile in Glas et al. (2025). Compound flood hazard scores were lowest across central and eastern Long Island, both south and north shores.





5 Discussion

450

455

The findings from this study demonstrate that there is quantifiable seasonality of compound coastal flood events across the study area (Fig. 3). For example, storm surges occur more frequently during the winter months when extratropical cyclones are at their strongest (Frame et al., 2017), which is a conclusion consistent with previous studies (e.g., Chen et al., 2024; Liu et al., 2020; Maduwantha et al., 2024) that characterized the temporal variability of coastal storm impacts in this area. For example, Chen et al. (2024) found that for stations surrounding New York City, tropical storms are associated with compound events with joint return periods of 50 years and higher, whereas extratropical cyclones tend to generate compound events with return periods of less than about 10 years. Booth et al. (2016) found that although hurricanes have historically created the conditions for the highest storm surge over

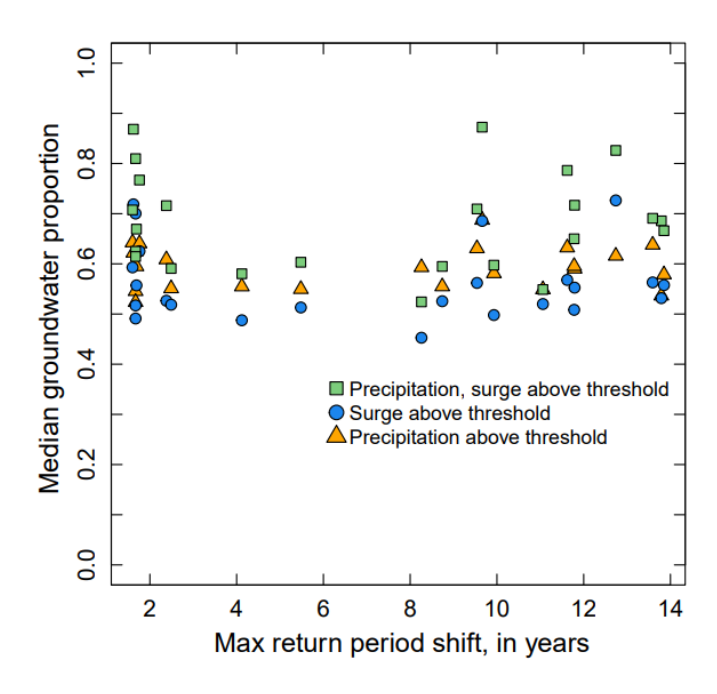


Figure 8. Median groundwater percentiles (based on the full monthly period of record during 1975–2021) during selected events: conditioned on precipitation (CoP), conditioned on surge (CoS), and during events where both variables exceeded their respective thresholds.

Public domain. CC0 1.0.



460

465

470

475

480



the past century along the mid-Atlantic and Northeastern U.S. coastline, moderate storms generated by extratropical cyclones have occurred more frequently, affect larger areas of coastline, and should not be ignored as important drivers of coastal flooding. In addition, the longer durations of extratropical cyclones than relatively short duration of tropical storms enhances the relative probability that extratropical cyclones will occur sometime during a high tide, whereas compound events generated by shorter duration, albeit more intense tropical systems, may miss the high tides entirely. For example, Marsooli and Wang (2020) found that if Post-Tropical Cyclone Sandy had arrived just 6 to 12 hours earlier, New York City would have experienced more severe flood impacts than those that occurred because it would have coincided with higher tides, along with variable effects from local bathymetry, coastal geometry, and floodwater speed.

The results of this study demonstrate relatively high dependence between daily precipitation and storm surge for both the south shore of Long Island and interior coastal Connecticut (Fig. 9a and 9b), which are areas exposed to storm tracks originating both on land and sea (Colle et al., 2010; Liu et al., 2021). Shallow depths to groundwater and substantial proportions of impervious area attributable to population density make coastal Connecticut and Long Island's south shore vulnerable to damages associated with all three drivers of compound flooding (Bjerklie et al., 2012; Walter et al., 2024). The regionally complex coastal geometry and bathymetry tends to enhance storm surge, mainly because of the relatively shallow continental shelf and low-level easterly winds (Bowman et al., 2013).

Additionally, Long Island's vulnerability to damages incurred by compound flooding is potentially exacerbated by factors such as the lack of protective dunes and expansive construction of coastal engineering infrastructure that inhibit the natural movement of beach sediment and increase the severity of beach erosion along the southwestern coast (Coch, 2015). Results from this study show that eastern Long Island, by contrast, showed both the lowest occurrence of compound events and also comprises more natural and agricultural land cover that potentially mitigate flood impacts compared to the more urbanized western part of the island (Glas et al., 2023). The potential for groundwater flooding was considered in this study, though data limitations restricted their direct integration into return period computations. However, the minimum monthly depth to groundwater serves as a valuable precondition for understanding the potential for groundwater flooding during precipitation-surge compound events.

Public domain. CC0 1.0.





Groundwater levels in the uppermost hydrogeologic units throughout the study area are highest (depth to water shallowest) in the winter (Barclay et al., 2024; Walter et al., 2024), when the likelihood of compound events is also highest. The connection between sea level rise forecasts (Shepard et al., 2012) and groundwater levels for coastal New York and Connecticut is not yet fully understood but will likely give rise to more dewatering demands for subsurface infrastructure and will likely interfere with natural drainage, exacerbating pluvial flooding (Masterson and Garabedian, 2007; Rosenzweig et al., 2024).





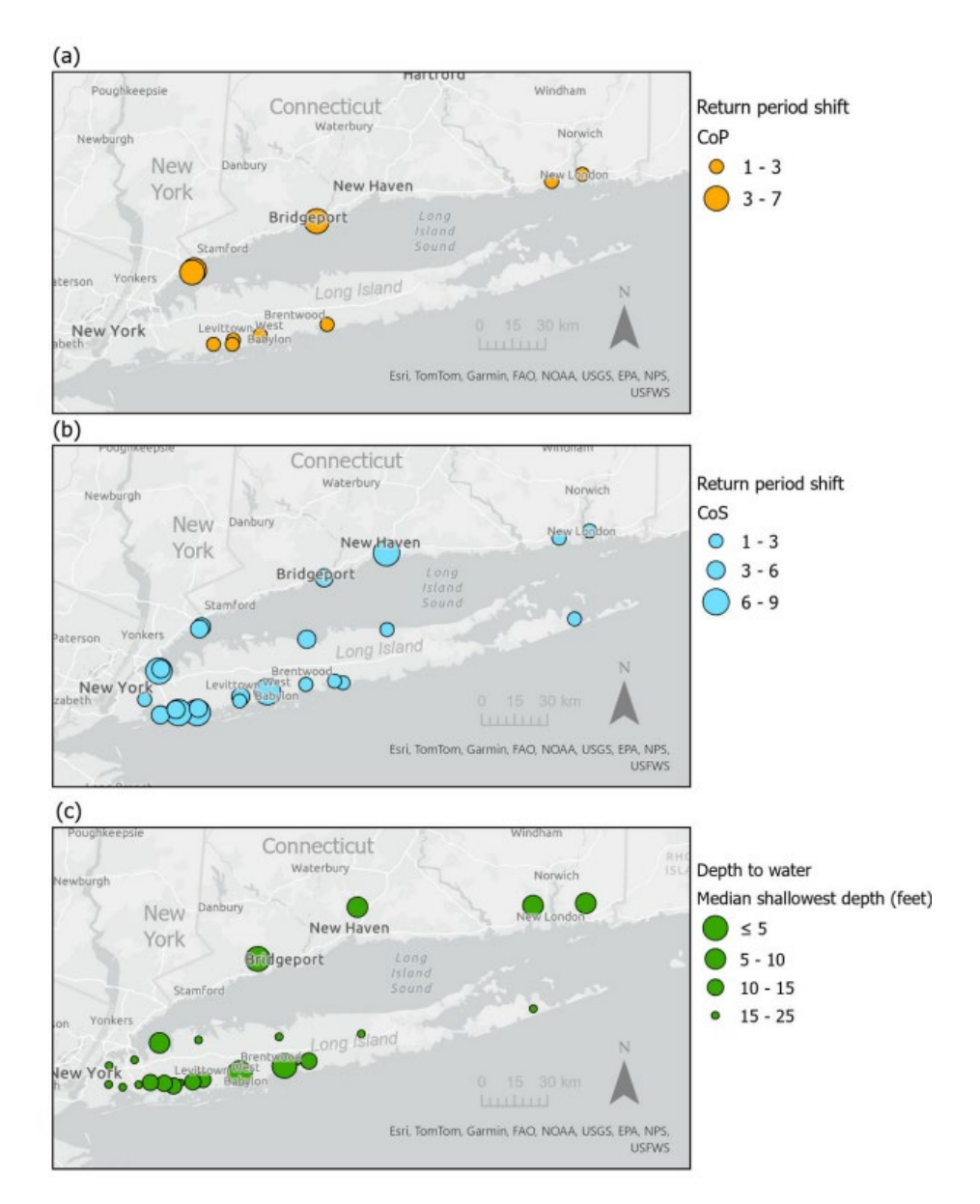


Figure 9. Maps of resulting compound flood hazard. (a) Return period shift for events exceeding threshold values in precipitation-conditioned (CoP) samples. The shift represents the factor difference between assumptions of dependence and independence, averaged using inverse 95% confidence interval weighting across several univariate return periods. (b) Return period shifts conditioned on surge (CoS). (c) Median shallowest groundwater depth (in feet) for well clusters located within the precipitation / surge search radius. Projection World Geodetic System of 1984, Base modified from U.S. Geological Survey digital data, 1:2,000,000.

Public domain. CC0 1.0.



495

500

505

510

515

520



5.1 Study Limitations

An important aspect of our results is their sensitivity to data quality, particularly in imputation techniques. Extreme values that have been estimated by imputation may be under-represented because of the tendency for regression to underpredict the variance of time series (Newman, 2014), potentially underestimating the true variability and risk of compound flooding. Imputation techniques that include a maintenance of variance (Vogel and Stedinger, 1985) may yield results that more accurately represent the variance of the system; however, these methods generally have lower predictive power than ordinary least squares or ridge regression (Levy et al., 2025) and should be used with caution if records show autocorrelation patterns typical of coastal water levels and groundwater (Matalas and Jacobs, 1964). Data imputation for this study is deemed prudent because imputation gains access to multiple stations throughout the study area that do not have complete data and have been traditionally left out of previous studies of compound flooding in the region (Ghanbari et al., 2021; Lai et al, 2021; Nasr et al., 2023; Wahl et al., 2015). Threshold selection approaches widely vary across the literature and can introduce variability in the results by influencing sample sizes and consequently the robustness of derived conclusions. Uncertainty associated with different threshold detection and declustering methods can be further increased under potentially nonstationary conditions (Agilan et al., 2021). Employing a variety of threshold selection techniques and investigating the sensitivity of results may be necessary to fully understand the spatial distribution of extreme events.

Multiple copula models were studied to understand precipitation-surge dependence better, limiting those models to two choices of elliptical copulas and four Archimedean types that may display tail dependence and such tail dependence in the appropriate tail (for this study the upper tail). These choices were based on previous studies (e.g., Phillips et al., 2022) and associated fit metrics for each copula choice. However, some studies have used a single copula model to describe a region so that the differences in dependence arise from the variability of parameter estimates instead of the practitioner's choice of copula model (e.g., Chen et al., 2024). This study incorporates elements of sampling and parameter uncertainty in the bootstrap procedure but does not address imputation uncertainty or model selection uncertainty. Ultimately, we chose not to implement a nonstationary copula model because

Public domain. CC0 1.0.





changes in tail dependence and overall correlation were judged as not substantial enough over the period of study to merit the introduction of additional uncertainty (Serinaldi and Kilsby, 2015).

6 Conclusion

525

530

535

540

An analysis of the co-occurrence of high precipitation, storm surge, and shallow groundwater depths was conducted across New York City, Long Island, and southern Connecticut to characterize the spatial distribution of compound flood potential. This study harnessed daily precipitation, storm surge, and monthly groundwater data from multiple stations, employing data imputation techniques to construct a more cohesive regional perspective on compound event occurrences than previous research. We applied bivariate joint probability copula models to estimate the frequency of potentially extreme precipitation-surge events, utilizing a biconditional sampling method that analyzes the extremes of each variable alongside the corresponding maximum precipitation or surge values over defined time lags.

We quantified the risk of compound event occurrences through a return period adjustment, representing the ratio of bivariate 'AND' return periods under independence versus dependence assumptions between precipitation and storm surge. A return period adjustment close to one indicates a minimal likelihood of compound events, while larger adjustments signify a substantially increased frequency when dependencies are considered. These adjustments are influenced by the univariate frequencies of interest. For instance, when assessing the co-occurrence probability of a 10-year precipitation event alongside a 10-year coastal event, the return period adjustment may reach a factor of 4. In contrast, for two 100-year events, this shift could soar to as high as 50. Notably, the univariate return periods are differentially adjusted, which in turn creates the curvature in the dependent return periods. To streamline these variations into a single representative value, we calculated a weighted





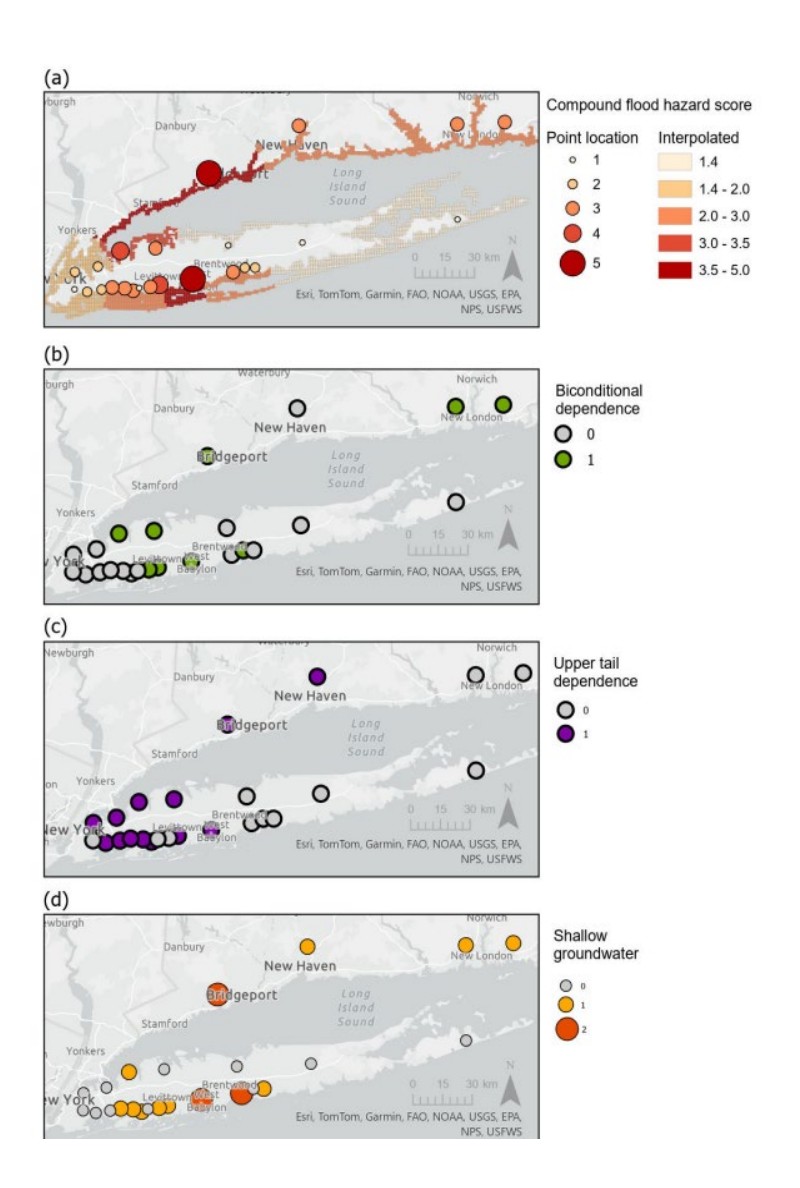


Figure 10. Breakdown of scoring assignments used to compute the compound flood hazard score. (a) Final hazard scores by triad. (b) One point assigned for biconditional dependence, defined as dependence in both rainfall-conditioned (CoP) and surge-conditioned (CoS) samples. (c) One point assigned if either CoP or CoS samples were best fit by a copula model exhibiting upper tail dependence. (d) Groundwater scores based on the median shallowest depth among selected wells per triad: 2 points for less than 6 ft below land surface (bls), 1 point for 6 to 15 ft bls, and 0 points for greater than 15 ft bls.

Public domain. CC0 1.0.



545

550

555

560

565



average of shifts, where the weights corresponded to the inverse of model variability derived from bootstrap-style resampling.

Results of this study show a regional gradient of compound event occurrence between precipitation and storm surge. Stronger dependence between flood drivers tends to occur in the southern part of Long Island, NNY and across interior coastal Connecticut. Smaller shift values were found for eastern Long Island and New York City. These differences are likely the result of interactions between storm tracks, coastal geometry, and local bathymetry that can enhance or amplify storm surges.

Although unconfined groundwater levels are shallow throughout the study area, they are most shallow in southern Nassau County, Long Island, which encompasses some of the higher return period adjustments and contribute to overall higher compound flood hazard scores (5 out of 5) than other station triads across the study area. Extremely shallow levels are also found in southwestern Connecticut. More study is required to evaluate the short-term response of groundwater to coastal and atmospheric extreme events in this region. Informed risk management is critical for effective coastal compound flood protection, particularly in regions like Long Island and Long Island Sound, where the interplay among groundwater, precipitation, and storm surge amplifies flood risk. Considering a combined framework that integrates these flood drivers together rather than in isolation could help increase understanding of hydrologic hazards in the study area. This approach is particularly important given the region's exposure to strong coastal storms and the presence of a dynamic shallow depth to groundwater, which can exacerbate flooding in urbanized and developing coastal zones. More work is needed across the region to examine process-based interactions of flood waters during compound events, extending the results of this study into site-specific interactions of subsurface infrastructure, groundwater dynamics and coastal processes in a coupled modelling framework for both present and future conditions.

Public domain. CC0 1.0.





Code and Data Availability

All data and R scripts supporting this study are archived in a U.S. Geological Survey data release (Glas et al., 2025). The release contains input files, both raw and imputed, scripts to replicate the analyses, and associated outputs to ensure full reproducibility.

570 Author contributions

R.G. led the Conceptualization, Methodology, Formal analysis, Visualization, and Writing – original draft. L.H. contributed to Conceptualization and Writing – review & editing. S.C. contributed to Data curation, Investigation, and Writing – review & editing. A.H. contributed to Data curation and Resources. K.M. contributed to Investigation and Writing – review & editing.

Acknowledgements

This work was supported by the U.S. Environmental Protection Agency Long Island Sound Study and by Hurricane Ida Supplemental appropriations. Any use of trade, firm, or product names is for descriptive purposes only and does not imply endorsement by the U.S. Government.

References

580

- Agel, L., Barlow, M., Qian, J. H., Colby, F., Douglas, E., & Eichler, T. (2015). Climatology of daily precipitation and extreme precipitation events in the northeast United States. Journal of Hydrometeorology, 16(6), 2537-2557. https://doi.org/10.1175/JHM-D-14-0147.1
- Agilan, V., Umamahesh, N. V., & Mujumdar, P. P. (2021). Influence of threshold selection in modeling peaks over threshold based nonstationary extreme precipitation series. Journal of Hydrology, 593, 125625. https://doi.org/10.1016/j.jhydrol.2020.125625
- Akaike, H. (1973). Maximum likelihood identification of Gaussian autoregressive moving average models. Biometrika, 60(2), 255–265. https://doi.org/10.1093/biomet/60.2.255



600

610



- Asquith, W.H., Kiang, J.E., and Cohn, T.A., 2017, Application of at-site peak-streamflow frequency analyses for very low annual exceedance probabilities: U.S. Geological Survey Scientific Investigation Report 2017–5038, 93 p., https://doi.org/10.3133/sir20175038.
 - Aurenhammer, F. (1991). Voronoi diagrams—a survey of a fundamental geometric data structure. *ACM computing surveys (CSUR)*, *23*(3), 345-405.
 - Barbot, S., Pineau-Guillou, L., & Delouis, J.-M. (2024). Extreme storm surge events and associated dynamics in the North Atlantic. Journal of Geophysical Research: Oceans, 129, e2023JC020772. https://doi.org/10.1029/2023JC020772
 - Barclay, J.R., Holland, M.J., and Mullaney, J.R., 2024, Simulated mean monthly groundwater-transported nitrogen loads in watersheds on the north shore of Long Island Sound, 1993–2022: U.S. Geological Survey Scientific Investigations Report 2024–5090, 63 p., https://doi.org/10.3133/sir20245090
 - Bjerklie, D.M., Mullaney, J.R., Stone, J.R., Skinner, B.J., and Ramlow, M.A., 2012, Preliminary investigation of the effects of sea-level rise on groundwater levels in New Haven, Connecticut: U.S. Geological Survey Open-File Report 2012–1025, 46 p., https://doi.org/10.3133/ofr20121025
- Booth, J. F., Rieder, H. E., & Kushnir, Y. (2016). Comparing hurricane and extratropical storm surge for the Mid-Atlantic and Northeast Coast of the United States for 1979–2013. Environmental Research Letters, 11(9), 094004. **DOI** 10.1088/1748-9326/11/9/094004
 - Bosserelle, A. L., Morgan, L. K., & Hughes, M. W. (2022). Groundwater rise and associated flooding in coastal settlements due to sea-level rise: a review of processes and methods. Earth's Future, 10(7), https://doi.org/10.1029/2021EF002580
 - Bowman, M. J., Colle, B. A., & Bowman, H. (2013). Storm surge modelling for the New York City region. In Climate Adaptation and Flood Risk in Coastal Cities (pp. 75–92). Routledge.
 - Brunner, M. I., Seibert, J., & Favre, A. C. (2016). Bivariate return periods and their importance for flood peak and volume estimation. Wiley Interdisciplinary Reviews: Water, 3(6), 819–833, https://doi.org/10.1002/wat2.1173



640



- Chen, Z., Orton, P., Booth, J., Wahl, T., DeGaetano, A., Kaatz, J., & Horton, R. (2024). Influence of storm type on compound flood hazard of a mid-latitude coastal-urban environment. Hydrology and Earth System Sciences Discussions, 2024, 1–30. https://doi.org/10.5194/hess-2024-135
- Coch, N. K. (2015). Unique vulnerability of the New York–New Jersey metropolitan area to hurricane destruction. Journal of Coastal Research, 31(1), 196–212.

https://doi.org/10.2112/JCOASTRES-D-13-00183.1

- Colle, B. A., Rojowsky, K., & Buonaito, F. (2010). New York City storm surges: Climatology and an analysis of the wind and cyclone evolution. Journal of Applied Meteorology and Climatology, 49(1), 85–100. https://doi.org/10.1175/2009JAMC2189.1
- Conestoga-Rovers and Associates, 2007. Revised Work Plan Vapor Intrusion Pathway Assessment, Bruno Cooperative Association, Associated Properties Superfund Site, Bruno, Nebraska, Consent Decree No. 8:02CV483. Accessed August 15, 2024 at https://semspub.epa.gov/work/07/30222021.pdf
- Cook, S.E. and Herdman, L.M., 2025, Geospatial dataset of coastal-inundation maps for Long Island and Long Island Sound (CT/NY): U.S. Geological Survey data release, https://doi.org/10.5066/P94P4WXX.
 - DeGaetano, A. T. (2008). Predictability of seasonal east coast winter storm surge impacts with application to New York's Long Island. Meteorological Applications, 15(2), 231–242. https://doi.org/10.1002/met.59
- Fallon, K., & Kuonen, J. (2023). Understanding Perceptions and Needs around Flooding and Erosion Risk for Shoreline Communities in Long Island and the Hudson River Estuary, New York. https://doi.org/10.25923/64hy-g695
 - Favre, A. C., El Adlouni, S., Perreault, L., Thiémonge, N., & Bobée, B. (2004). Multivariate hydrological frequency analysis using copulas. Water Resources Research, 40(1). https://doi.org/10.1029/2003WR002456
 - Forman, A. (2014). Caution Ahead: Overdue Investments for New York's Aging Infrastructure. Center for an Urban Future. https://eric.ed.gov/?id=ED555648



650

655



- Frame, T., Harrison, G., Hewson, T., & Roberts, N. (2017). Meteorological risk: Extra-tropical cyclones, tropical cyclones and convective storms. In K. Poljanšek, M. Marin Ferrer, T. De Groeve, & I. Clark (Eds.), Science for disaster risk management 2017: Knowing better and losing less (pp. 246–256). Publications Office of the European Union. https://doi.org/10.2760/17520
- Genest, C. and A. C. Favre (2007). Everything you always wanted to know about copula modeling but were afraid to ask. Journal of Hydrologic Engineering, 12 (4), 347–368. https://doi.org/10.1061/(ASCE)1084-0699(2007)12:4(347)
- Ghanbari, M., Arabi, M., Kao, S. C., Obeysekera, J., & Sweet, W. (2021). Climate change and changes in compound coastal-riverine flooding hazard along the US coasts. Earth's Future, 9(5), e2021EF002055. https://doi.org/10.1029/2021EF002055
- Glas, R., Hecht, J., Simonson, A., Gazoorian, C., & Schubert, C. (2023). Adjusting design floods for urbanization across groundwater-dominated watersheds of Long Island, NY. Journal of Hydrology, 618, 129194. https://doi.org/10.1016/j.jhydrol.2023.129194
- Glas, R., Herdman, L., Cook, S., Masterson, K., 2025, Supporting Datasets and R Code for Compound Flood Hazard Modeling in the New York Long Island Sound Region. U.S. Geological Survey data release, https://doi.org/10.5066/P13ARD2K.
- Green, J., Haigh, I. D., Quinn, N., Neal, J., Wahl, T., Wood, M., Eilander, D., de Ruiter, M., Ward, P., and Camus, P., (2024). A comprehensive review of coastal compound flooding literature. arXiv preprint arXiv:2404.01321.https://doi.org/10.48550/arXiv.2404.01321
 - Hanchey A, Schnall A, Bayleyegn T, et al. *Notes from the Field:* Deaths Related to Hurricane Ida Reported by Media Nine States, August 29–September 9, 2021. MMWR Morb Mortal Wkly Rep 2021;70:1385–1386. DOI: http://dx.doi.org/10.15585/mmwr.mm7039a3
 - Herreros-Cantis, P., Olivotto, V., Grabowski, Z. J., & McPhearson, T. (2020). Shifting landscapes of coastal flood risk: Environmental (in) justice of urban change, sea level rise, and differential vulnerability in New York City. Urban Transformations, 2(1), 9, https://doi.org/10.1186/s42854-020-00014-w





- Huang, W., & Prokhorov, A. (2014). A goodness-of-fit test for copulas. Econometric Reviews, 33(7), 751–771. https://doi.org/10.1080/07474938.2012.690692
 - Jane, R., Cadavid, L., Obeysekera, J., and Wahl, T. (2020). Multivariate statistical modelling of the drivers of compound flood events in South Florida, Nat. Hazards Earth Syst. Sci., 20, 2681– 2699, https://doi.org/10.5194/nhess-20-2681-2020.
- Jane, R.A., Malagón-Santos, V., Rashid, M.M., Doebele, L., Wahl, T., Timmers, S.R., Serafin, K.A., Schmied, L. and Lindemer, C., 2022. A hybrid framework for rapidly locating transition zones: A comparison of event-and response-based return water levels in the Suwannee River FL. Water Resources Research, 58(11), p.e2022WR032481. https://doi.org/10.1029/2022WR032481
- Kouhi, S., Hashemi, M. R., Spaulding, M., & Hara, T. (2022). Modeling the impact of sea level rise on maximum water elevation during storm surge events: a closer look at coastal embayments. Climatic Change, 171(3), 31. https://doi.org/10.1007/s10584-022-03342-x
 - Kunkel, K. E., Karl, T. R., Squires, M. F., Yin, X., Stegall, S. T., & Easterling, D. R. (2020).

 Precipitation extremes: Trends and relationships with average precipitation and precipitable water in the contiguous United States. Journal of Applied Meteorology and Climatology, 59(1), 125–142. https://doi.org/10.1175/JAMC-D-19-0185.1
 - Lai, Y., Li, J., Gu, X., Liu, C., & Chen, Y. D. (2021). Global compound floods from precipitation and storm surge: Hazards and the roles of cyclones. Journal of Climate, 34(20), 8319–8339. https://doi.org/10.1175/JCLI-D-21-0050.1
- 690 Liu, C., Onat, Y., Jia, Y., & O'Donnell, J. (2021). Modeling nearshore dynamics of extreme storms in complex environments of Connecticut. *Coastal Engineering*, 168, 103950.
 https://doi.org/10.1016/j.coastaleng.2021.103950
 - Levy, Z. F., Glas, R. L., Stagnitta, T. J., & Terry, N. (2025). ARCHI: A New R Package for Automated Imputation of Regionally Correlated Hydrologic Records. Groundwater. https://doi.org/10.1111/gwat.13474





- Levy, Z. F., Stagnitta, T. J., and Glas, R. L., 2024, ARCHI: Automated Regional Correlation Analysis for Hydrologic Record Imputation, v1.0.0: U.S. Geological Survey software release, https://doi.org/10.5066/P1VVHWKE.
- Li, B., Rodell, M., & Famiglietti, J. S. (2015). Groundwater variability across temporal and spatial scales in the central and northeastern US. Journal of Hydrology, 525, 769–780. https://doi.org/10.1016/j.jhydrol.2015.04.033
 - Liu, C., Jia, Y., Onat, Y., Cifuentes-Lorenzen, A., Ilia, A., McCardell, G., Fake, T., & O'Donnell, J. (2020). Estimating the Annual Exceedance Probability of Water Levels and Wave Heights from High Resolution Coupled Wave-Circulation Models in Long Island Sound. *Journal of Marine Science and Engineering*, 8(7), 475. https://doi.org/10.3390/jmse8070475
 - Maduwantha, P., Wahl, T., Santamaria-Aguilar, S., Jane, R., Booth, J. F., Kim, H., and Villarini, G.: A multivariate statistical framework for mixed storm types in compound flood analysis, Nat. Hazards Earth Syst. Sci., 24, 4091–4107, https://doi.org/10.5194/nhess-24-4091-2024, 2024.
- Marsooli R and Wang Y (2020) Quantifying tidal phase effects on coastal flooding induced by

 Hurricane Sandy in Manhattan, New York using a micro-scale hydrodynamic model. Front.

 Built Environ. 6:149. doi: 10.3389/fbuil.2020.00149
 - Masterson, J. P., & Garabedian, S. P. (2007). Effects of sea-level rise on ground water flow in a coastal aquifer system. *Groundwater*, 45(2), 209-217.
 - Matalas, N.C., and Jacobs, B.A., (1964), A correlation procedure for augmenting hydrologic data. U.S. Geological Survey Professional Paper 434-E, 7p. https://doi.org/10.3133/pp434E
 - MacQueen, J.: Some methods for classification and analysis of multivariate observations, in:

 Proceedings of the Fifth Berkeley Symposium on Mathematical Statistics and Probability,

 Volume 1: Statistics, edited by: Cam, L. M. L. and Neyman, J., University of California Press,

 281–297, 1967.
- Nagler, T., Schepsmeier, U., Stoeber, J., Brechmann, E.C., Graeler, B., Erhardt, T., Almeida, C., Min, A., Czado, C., Hofmann, M., Killiches, M., Joe, H., & Vatter, T. (2023), VineCopula: statistical inference of vine copulas, https://doi.org/10.32614/CRAN.package.VineCopula version 2.5.0, dated July 10, 2023





- Nasr, A. A., Wahl, T., Rashid, M. M., Jane, R. A., Camus, P., & Haigh, I. D. (2023). Temporal changes in dependence between compound coastal and inland flooding drivers around the contiguous United States coastline. Weather and Climate Extremes, 41, 100594. https://doi.org/10.1016/j.wace.2023.100594
 - Nederhoff, K., Leijnse, T. W., Parker, K., Thomas, J., O'Neill, A., van Ormondt, M., McCall, R., Erikson, L., Barnard, P.L., Foxgrover, A., & Klessens, W. (2024). Tropical or extratropical cyclones: what drives the compound flood hazard, impact, and risk for the United States Southeast Atlantic coast?. Natural Hazards, pp.1–47. https://doi.org/10.1007/s11069-024-06552-x
 - New Jersey Department of Environmental Protection, 2021. Vapor Intrusion Technical Guidance Version 5.0. Accessed August 15, 2024 at https://dep.nj.gov/srp/guidance/vapor-intrusion/
- Newman, D. A. (2014). Missing data: Five practical guidelines. Organizational research methods, 17(4), 372–411. https://doi.org/10.1177/1094428114548590
 - NOAA Center for Operational Oceanographic Products and Services (CO-OPS). (2023). *Tides & Currents: Water Level Observations* [Data set]. National Oceanic and Atmospheric Administration, U.S. Department of Commerce. Retrieved October 1, 2023, from https://tidesandcurrents.noaa.gov
 - NOAA National Centers for Environmental Information (NCEI). (2023). *Daily Summaries: Global Historical Climatology Network (GHCN-Daily)* [Data set]. U.S. Department of Commerce. Retrieved October 1, 2023, from https://www.ncei.noaa.gov
- O'Donnell, J., & O'Donnell, J. E. (2012). Coastal vulnerability in Long Island Sound: The spatial structure of extreme sea level statistics. In 2012 Oceans (pp. 1–4). IEEE.

 10.1109/OCEANS.2012.6405099
 - Orton, P., Georgas, N., Blumberg, A., & Pullen, J. (2012). Detailed modeling of recent severe storm tides in estuaries of the New York City region. Journal of Geophysical Research: Oceans, 117(C9). https://doi.org/10.1029/2012JC008220
- Pedregosa, F., Varoquaux, G., Gramfort, A., Michel, V., Thirion, B., Grisel, O., Blondel, M.,
 Prettenhofer, P., Weiss, R., Dubourg, V., Vanderplas, J., Passos, A., Cournapeau, D., Brucher,





- M., Perrot, M., and Duchesnay, É.: Scikit-learn: Machine Learning in Python, J. Mach. Learn. Res., 12, 2825–2830, 2011.
- Phillips, R. C., Samadi, S., Hitchcock, D. B., Meadows, M. E., & Wilson, C. A. M. E. (2022). The devil is in the tail dependence: An assessment of multivariate copula-based frameworks and dependence concepts for coastal compound flood dynamics. Earth's Future, 10(9), e2022EF002705. https://doi.org/10.1029/2022EF002705
 - R Core Team. (2024). *R: A language and environment for statistical computing*. R Foundation for Statistical Computing, Vienna, Austria. https://www.R-project.org/
 - Rosenzweig, B., Montalto, F. A., Orton, P., Kaatz, J., Maher, N., Kleyman, J. et al. (2024). NPCC4: Climate Change and New York City's Flood Risk. Annals of the New York Academy of Sciences, 1539, 127-184.https://doi.org/10.1111/nyas.15175
 - Salvadori, G. (2004). Bivariate return periods via 2-copulas. Statistical Methodology, 1(1-2), 129–144. https://doi.org/10.1016/j.stamet.2004.07.002
 - Salvadori, G., & De Michele, C. (2007). On the use of copulas in hydrology: Theory and practice. Journal of Hydrologic Engineering, 12(4), 369–380. https://doi.org/10.1061/(ASCE)1084-0699(2007)12:4(369">https://doi.org/10.1061/(ASCE)1084-0699(2007)12:4(369">https://doi.org/10.1061/(ASCE)1084-0699(2007)12:4(369")
- Salvadori, G., & De Michele, C. (2010). Multivariate multiparameter extreme value models and return periods: A copula approach. Water Resources Research,

 46(10). https://doi.org/10.1029/2009WR009040
 - Serinaldi, F., & Kilsby, C. G. (2015). Stationarity is undead: Uncertainty dominates the distribution of extremes. Advances in Water Resources, 77, 17–36. https://doi.org/10.1016/j.advwatres.2014.12.013
- Shepard, C. C., Agostini, V. N., Gilmer, B., Allen, T., Stone, J., Brooks, W., & Beck, M. W. (2012).

 Assessing future risk: quantifying the effects of sea level rise on storm surge risk for the southern shores of Long Island, New York. Natural Hazards, 60, 727–745.

 https://doi.org/10.1007/s11069-011-0046-8



790



- Shiau, J. T. (2003). Return period of bivariate distributed extreme hydrological events. Stochastic

 Environmental Research and Risk Assessment, 17, 42–57. https://doi.org/10.1007/s00477-003-0125-9
 - Strauss, B. H., Orton, P. M., Bittermann, K., Buchanan, M. K., Gilford, D. M., Kopp, R. E., Kulp, S., Massey, C., de Moel, H., & Vinogradov, S. (2021). Economic damages from Hurricane Sandy attributable to sea level rise caused by anthropogenic climate change. Nature Communications, 12, 2720. https://doi.org/10.1038/s41467-021-22838-1
 - Su, X., Belvedere, P., Tosco, T., & Prigiobbe, V. (2022). Studying the effect of sea level rise on nuisance flooding due to groundwater in a coastal urban area with aging infrastructure. Urban Climate, 43, 101164. https://doi.org/10.1016/j.uclim.2022.101164
 - Suffolk County DMA 2000 Hazard Mitigation Plan Update Suffolk County, New York, section 5.4.15: shallow groundwater flooding, 2020.

 https://www.southamptontownny.gov/DocumentCenter/View/24204/Section-5415---Shallow-GW-Flooding
 - U.S. Geological Survey, 2023, USGS water data for the Nation: U.S. Geological Survey National Water Information System database, accessed June 8, 2023, at https://doi.org/10.5066/F7P55KJN.
 - U.S. Census Bureau. (2023). *County Population Totals: 2020–2024*. Table CO-EST2023-POP, U.S. Department of Commerce. Retrieved [11 1, 2023], from: https://www.census.gov/data/tables/time-series/demo/popest/2020s-counties-total.html
- Vogel, R. M., & Stedinger, J. R. (1985). Minimum variance streamflow record augmentation procedures. Water Resources Research, 21(5), 715–723. https://doi.org/10.1029/WR021i005p00715
 - Wahl, T., Jain, S., Bender, J., Meyers, S. D., & Luther, M. E. (2015). Increasing risk of compound flooding from storm surge and precipitation for major US cities. Nature Climate Change, 5(12), 1093–1097. https://doi.org/10.1038/nclimate2736
- Walter, D.A., Jahn, K.L., Masterson, J.P., Dressler, S.E., Finkelstein, J.S., and Monti, J., Jr., 2024, Simulation of groundwater flow in the Long Island, New York regional aquifer system for





- pumping and recharge conditions from 1900 to 2019: U.S. Geological Survey Scientific Investigations Report 2024–5044, 113 p., https://doi.org/10.3133/sir20245044.
- Welk, R.J., Masterson, K.K, Barclay, J.R., and Jahn, K.L., 2025a, Geospatial datasets of factors influencing groundwater emergence flood hazard in Long Island, New York and near coastal areas surrounding Long Island Sound in New York, Connecticut, and Rhode Island: U.S. Geological Survey data release, https://doi.org/10.5066/P9W4QIV5.
- Welk, R.J., Fisher, B.N., Glas, R.L., Herdman, L.M., Jahn, K.L., Masterson, K.K., 2025b, Geospatial datasets of factors influencing pluvial flood potential in Long Island, New York and near coastal areas surrounding Long Island Sound in New York, Connecticut, and Rhode Island. U.S. Geological Survey data release, https://doi.org/10.5066/10.5066/P9N6J1SN.
- Wong, K. C. (1990). Sea level variability in Long Island Sound. Estuaries, 13, 362–372. https://doi.org/10.2307/1351781
- Zscheischler, J., & Seneviratne, S. I. (2017). Dependence of drivers affects risks associated with compound events. Science advances, 3(6), DOI: 10.1126/sciadv.1700263 820

Public domain. CC0 1.0.





Triad	Station ID _{pcpt}	Long _{pcpt}	Latpcpt	Station ID _{coastal}	Agency _{coastal}	Longcoastal	Lat _{coastal}	$Gw_{\text{rad, km}}$	Gw_{nwells}	Long _{GW}	Lat _{GW}	Map ID
1	USW00094789	-73.7639	40.6392	01311875	USGS	-73.885136	40.57371636	8	3	40.66038142	-73.85207963	R1- C1
2	USW00094789	-73.7639	40.6392	01311850	USGS	-73.7579103	40.6173266	6	2	40.67038128	-73.7869389	R1- C2
3	USW00014732	-73.8803	40.7794	8516945	NOAA	-73.7650033	40.80999678	5	3	40.77248147	-73.80349073	R2- C3
4	USW00014732	-73.8803	40.7794	8516990	NOAA	-73.78166929	40.79333757	9	2	40.74863888	-73.90804169	R2- C4
5	USW00094789	-73.7639	40.6392	01310521	USGS	-73.5754058	40.6276026	5	2	40.66530555	-73.64354169	R1- C5
6	USW00094789	-73.7639	40.6392	01310740	USGS	-73.5837396	40.5934366	8	3	40.67594172	-73.68191403	R1- C6
7	USW00094789	-73.7639	40.6392	01311145	USGS	-73.7373543	40.59316026	9	4	40.67966767	-73.7386687	R1- C7
8	USW00054787	-73.4164	40.7344	01310521	USGS	-73.5754058	40.6276026	6	2	40.69148991	-73.52373709	R3- C5
9	USW00054787	-73.4164	40.7344	01310740	USGS	-73.5837396	40.5934366	13	2	40.68242593	-73.56518865	R3- C6
10	USW00054787	-73.4164	40.7344	01311145	USGS	-73.7373543	40.59316026	6	6	40.67746142	-73.61586381	R3- C7
11	USC00067970	-73.5475	41.1247	8516945	NOAA	-73.7650033	40.80999678	15	4	40.84183701	-73.70124159	R4- C3
12	USC00067970	-73.5475	41.1247	8516990	NOAA	-73.78166929	40.79333757	22	3	40.85384259	-73.54185187	R4- C4
13	USC00063207	-72.0378	41.3503	01194796	USGS	-72.3459166	41.3125983	18	2	41.40519723	-72.17144725	R5- C8
14	USC00063207	-72.0378	41.3503	8461490	NOAA	-72.09499657	41.37167072	23	2	41.41445834	-71.95556669	R5- C9
15	USW00094789	-73.7639	40.6392	8518750	NOAA	-74.0150011	40.70000404	5	8	40.67155779	-73.90988824	R1- C10
16	USW00054787	-73.4164	40.7344	01309225	USGS	-73.3556765	40.66926687	5	4	40.717625	-73.37287499	R3- C11
17	USW00004781	-73.1019	40.7939	01309225	USGS	-73.3556765	40.66926687	5	2	40.74805554	-73.1894861	R6- C11
18	USW00054790	-72.8675	40.8211	01309225	USGS	-73.3556765	40.66926687	5	2	40.76749999	-73.1363472	R7- C11
19	US1NYSF0123	-72.7981	40.8068	01309225	USGS	-73.3556765	40.66926687	8	3	40.76776851	-73.08955553	R8- C11
20	USC00300889	-72.2978	40.9519	8510560	NOAA	-71.95930163	41.04812618	5	3	40.98185951	-72.17026343	R9- C12
21	USC00301309	-73.3731	40.8833	8514560	NOAA	-73.07666422	40.95000233	8	2	40.86670833	-73.21156945	R10- C13
22	USC00307134	-72.7161	40.9625	8514560	NOAA	-73.07666422	40.95000233	12	2	40.879	-72.87479165	R11- C13
23	USW00094702	-73.1267	41.1642	8467150	NOAA	-73.18166364	41.1733364	13	4	41.18623542	-73.2990625	R12- C14
24	USW00014758	-72.8892	41.2589	8465705	NOAA	-72.9083334	41.28333752	15	3	41.39843517	-72.89087036	R13- C15

Table 1. Station triad locations and associated precipitation (pcpt) and coastal station identification numbers (Station ID), including Map IDs referenced in Fig. 1. Agency operating each coastal station indicated as either U.S. Geological Survey (USGS) or National Oceanic and Atmospheric Administration (NOAA) indicated as Agency_{coastal}. Each triad consists of a National Oceanic and Atmospheric Administration (NOAA) precipitation gage (NOAA NCEI, 2023), a U.S. Geological Survey (2023) or NOAA tidal station (NOAA CO-OPS, 2023), and the centroid of a number of clustered groundwater observation wells (GWnwells, U.S. Geological Survey, 2023) selected within the search radius in kilometers (GWrad,km) centered on the precipitation—tidal station midpoint.

Public domain. CC0 1.0.





	RMSE	Average Bias				
PPT_{wet}	8.96 mm	-1.49 mm				
PPT* _{dry}	1.66 mm	0.34 mm				
PPT* _{all}	4.59 mm	-0.08 mm				
NTR	0.09 m	-0.0011 m				
GW	1.1 ft	-0.0012 ft				

^{*}ARCHI imputed values have been censored such that values less than 1mm are forced to zero.

Table 2. Imputation performance statistics from a 5% holdout analysis conducted separately for wet days (precipitation (PPT) > 1 mm) and dry days (precipitation = 0 mm). Metrics include root mean square error (RMSE) and percent bias between withheld and imputed values. Results are shown for daily nontidal residual (NTR, in meters) and monthly depth to groundwater (GW, in feet).





Triad	Thr _{pcpt}	N _{CoP}	Tau_{CoP}	Pcorr _{CoP}	EPY _{pcpt}	Thr_{SG}	N _{CoS}	Tau _{CoS}	Pcorr _{CoS}	EPY_{SG}
1	0.99	167	0.069	0.19	3.21	0.98	201	0.12	0.012	3.87
2	0.99	167	0.08	0.12	3.21	0.98	201	0.13	0.0062	3.87
3	0.99	169	0.077	0.14	3.25	0.98	202	0.12	0.009	3.88
4	0.99	169	0.069	0.19	3.25	0.97	265	0.16	0.00017	5.1
5	0.99	167	0.065	0.21	3.21	0.98	198	0.12	0.01	3.81
6	0.99	167	0.066	0.21	3.21	0.97	272	0.12	0.0033	5.23
7	0.99	167	0.069	0.19	3.21	0.97	268	0.11	0.01	5.15
8	0.98	296	0.092	0.018	5.69	0.98	198	0.11	0.019	3.81
9	0.98	296	0.088	0.025	5.69	0.98	199	0.11	0.017	3.83
10	0.98	296	0.083	0.033	5.69	0.98	200	0.09	0.058	3.85
11	0.98	298	0.092	0.018	5.73	0.98	202	0.11	0.023	3.88
12	0.98	298	0.087	0.025	5.73	0.97	265	0.18	1.30E-05	5.1
13	0.98	305	0.081	0.034	5.87	0.97	271	0.16	7.60E-05	5.21
14	0.98	305	0.077	0.045	5.87	0.97	286	0.14	0.00034	5.5
15	0.99	167	0.077	0.14	3.21	0.98	201	0.13	0.0046	3.87
16	0.98	296	0.094	0.016	5.69	0.97	268	0.14	0.00092	5.15
17	0.99	170	-0.019	0.72	3.27	0.97	268	0.11	0.0052	5.15
18	0.98	296	0.092	0.018	5.69	0.97	268	0.16	9.90E-05	5.15
19	0.98	297	-0.041	0.29	5.71	0.97	268	0.17	4.10E-05	5.15
20	0.98	301	-0.052	0.18	5.79	0.97	272	0.098	0.016	5.23
21	0.98	298	0.019	0.62	5.73	0.97	271	0.17	2.80E-05	5.21
22	0.98	308	0.051	0.19	5.92	0.97	271	0.19	3.60E-06	5.21
23	0.99	162	0.11	0.04	3.12	0.98	202	0.14	0.0043	3.88
24	0.99	164	0.05	0.35	3.15	0.97	270	0.12	0.0032	5.19

Table 3. Summary of biconditional samples for rainfall and coastal storm surge. The table includes selected threshold quantiles (Thr), Kendall's tau correlation coefficients (Tau) and corresponding p-values (Pcorr), and the average number of events per year (EPY). Values are shown for precipitation (pcpt), surge (SG), and the number (N) of bivariate events conditioned on precipitation (CoP) and conditioned on surge (CoS). Bold P values indicate tau is significant.

Public domain. CC0 1.0.





		Conditioned on Rain	Conditioned on Surge							
Triad	Copula family	Parameter estimate	P_{GOF}	ΔΑΙС	ΔuTDC	Copula family	Parameter estimate	P_{GOF}	ΔΑΙС	ΔuTDC
1	Independence	-	-	-	-	Gumbel	1.1	0.22	0	0.082
2	Independence	-	-	-	-	Survival Clayton	0.27	0.96	0	0.067
3	Independence	-	-	-	-	Survival Clayton	0.29	0.52	0	0
4	Independence	-	-	-	-	Survival Clayton	0.35	0.5	0.37	0.085
5	Independence	-	-	-	-	Survival Clayton	0.27	0.8	0	0.056
6	Independence	-	-	-	-	Gumbel	1.1	0.98	0	0.028
7	Independence	-	-	-	-	Gumbel	1.1	0.72	0	0.056
8	Gaussian	0.16	0.51	0	0.083	Survival Clayton	0.23	0.39	0	0.049
9	Gaussian	0.16	0.63	0	0.083	Frank	1	0.64	0.27	0
10	Gaussian	0.15	0.65	0	0.083	Independence	-	-	-	-
11	Gumbel	1.1	0.55	0	0.056	Gumbel	1.1	0.73	0	0.046
12	Survival Clayton	0.19	0.56	0	0	Gaussian	0.29	0.29	0	0.11
13	Frank	0.72	0.76	0	0.062	Frank	1.5	0.67	1.3	0.077
14	Frank	0.68	0.4	0	0.062	Frank	1.3	0.18	0	0.071
15	Independence	-	-	-	-	Gaussian	0.23	0.12	0	0
16	Gaussian	0.17	0.9	0	0.083	Gumbel	1.1	0.32	0	0.082
17	Independence	-	-	-	-	Frank	1.1	0.91	0	0.082
18	Frank	0.83	0.33	0	0.067	Frank	1.5	0.41	0	0
19	Independence	-	-	-	-	Frank	1.6	0.15	0	0
20	Independence	-	-	-	-	Frank	0.89	0.65	0	0.009
21	Independence	-	-	-	-	Gaussian	0.26	0.9	0	0.043
22	Independence	-	-	-	-	Frank	1.7	0.53	0	0.006
23	Survival Clayton	0.21	0.57	0.58	0	Gumbel	1.2	0.15	0	0
24	Independence	-	-	-	-	Gumbel	1.1	0.23	0	0.09

Table 4. Selected copula models and their corresponding parameter estimates, along with ΔAIC and $\Delta uTDC$ values used in the model selection process. $\Delta uTDC$ represents the difference between the empirical upper tail dependence coefficient and the median of the bootstrapped fitted model estimates. P values are presented for the semi-parametric goodness of fit test (P_{GOF} , Huang and Prokhorov, 2014). Dashes indicate that independence copula was fit and no parameters are applicable.







Triad	RPshift _{CoP}	$RPshift_{CoS}$	Med_{GW}	GW score	Biconditional Dependence Score	Upper Tail Dependence Score	Component Score Sum	Final Hazard Score
1		5.62	15.76	0	0	1	1	2
2		5.47	15.46	0	0	1	1	2
3		5.84	21	0	0	1	1	2
4		8.51	15.755	0	0	1	1	2
5		5.33	13.955	1	0	1	2	3
6		7.43	13.63	1	0	1	2	3
7		7	11.6	1	0	1	2	3
8	2.45	4.67	13.64	1	1	1	3	4
9	2.38	1.55	11.215	1	1	0	2	3
10	2.33		16.1	0	0	0	0	1
11	6.86	5	8.405	1	1	1	3	4
12	5.48	3.82	18.78	0	1	1	2	3
13	1.37	1.86	7.805	1	1	0	2	3
14	1.37	1.76	7.82	1	1	0	2	3
15		2.76	15.9	0	0	0	0	1
16	2.48	7.38	4.015	2	1	1	4	5
17		1.57	1.77	2	0	0	2	3
18	1.45	1.85	19.365	0	1	0	1	2
19		1.92	14.73	1	0	0	1	2
20		1.47	18.64	0	0	0	0	1
21		3.56	17.855	0	0	0	0	1
22		2.01	24.735	0	0	0	0	1
23	3.74	5.94	1.835	2	1	1	4	5
24		7.05	9.07	1	0	1	2	3

Table 5. Summary of average return period shifts for rain–surge events conditioned on precipitation (CoP) and on surge (CoS), along with the median shallowest depth to groundwater (MedGW, in feet) for each well cluster associated with a triad. Component-based scores for groundwater depth, biconditional dependence, and upper tail dependence were summed and scaled to produce an integrated composite hazard rating (Final Hazard Score). Data available in Glas et al. (2025).